

LOG FOCAL FREQUENCY LOSS FOR BIOIMAGE RESTORATION

Xingjian Zhang^{*†} Claire Leclech^{*} Louison Blivet-Bailly^{*}
Abdul I. Barakat^{*} Elsa D. Angelini[†]

^{*} LadHyX, CNRS, École polytechnique, Institut Polytechnique de Paris, France

[†] LTCI, Télécom Paris, Institut Polytechnique de Paris, France

ABSTRACT

Image restoration of biological structures in microscopy poses unique challenges for preserving fine textures and sharp edges. While recent GAN-based image restoration formulations have introduced frequency-domain losses for natural images, microscopy images pose distinct challenges with large dynamic ranges and sparse but critical structures with spatially-variable contrast. Inspired by the principle of logarithmic perception in human vision, we propose a log focal frequency loss (LFFL) tailored for microscopy restoration. This loss combines adaptive spectral weighting from log-space differences with log-dampened error measurement, ensuring balanced reconstruction across all frequency bands while preserving both structural coherence and fine details. We tested our GAN-based framework on two use-cases with real ground-truths: deblurring of fluorescence images of cell nuclei on microgroove substrates and denoising of zebrafish embryo images from the FMD dataset. Compared to training with only spatial-domain losses and with existing frequency-domain losses, our method achieves improvements across several quality metrics. Code is available at github.com/xjzhaang/log-focal-frequency-loss.

Index Terms— image restoration, GAN, fluorescence microscopy, frequency domain loss, deblurring, denoising

1. INTRODUCTION

Fluorescence microscopy images are frequently blurry, out-of-focus, or noisy due to optical limitations, specimen thickness, or suboptimal imaging conditions. Deep learning-based image denoising and deblurring methods have become powerful tools for enhancing image quality, yet they face a fundamental limitation: neural networks trained with gradient descent exhibit spectral bias [1]—an inherent bias toward learning low-frequency components while struggling to capture high-frequency details. Spatial losses fail to counteract this limitation as they uniformly average errors across pixels, diluting gradients of high-frequency features. While current frequency-domain formulations explicitly target spectral content, they typically rely on raw frequency amplitudes [2, 3]

where larger low-frequency amplitudes disproportionately influence the loss. This limitation is particularly problematic for fluorescence microscopy images which often contain only sparse bright structures against low-intensity backgrounds. Meaningful information primarily resides in high-frequency components representing edges and fine textures, but the foreground-background imbalance compounds spectral bias, rendering high-frequency restoration even more challenging. To address this gap, we propose a log focal frequency loss that re-balances learning across frequency scales into a standard GAN-based framework. We introduce a logarithmic focal weight and a log-dampened error to equalize the relative contributions of different frequency components.

1.1. Related Work

Classical image restoration losses, such as pixel-wise L1 or L2 norms, prioritize overall intensity accuracy and tend to suppress fine details such as edges and textures [4]. Perceptual losses based on deep feature activations improve semantic fidelity [5], yet in microscopy images they remain biased toward background regions, as spatial averaging dilutes the contribution of localized biologically-relevant structures.

Recent frequency-domain approaches for image reconstruction include neural network architectures that explicitly process spectral representations [6, 7] and loss formulations that operate in the frequency domain [2, 3], often to address the inherent spectral bias of neural networks toward learning low-frequency components [1]. Specific frequency-domain losses have decomposed the problem in various ways. Fuoli et al. [2] proposed the Fourier Space Loss (FSL), which separately computes L1 losses on amplitude and phase components of the Fourier transform. Focal Frequency Loss (FFL) [3] took a different approach, introducing adaptive weighting based on frequency-wise errors to dynamically emphasize harder-to-learn frequencies. However, both approaches do not account for the fact that the amplitudes of low-frequency components can be orders of magnitude larger than those of high frequencies, causing their losses to be disproportionately weighted toward low-frequency regions.

2. METHODS

2.1. Log Focal Frequency Loss

We propose a weighted log frequency loss tailored to microscopy images, building upon the FFL framework introduced in [3] for natural image reconstruction and synthesis. We modify this framework by introducing logarithmic scaling at two stages: (1) computing adaptive weights from log differences of real and imaginary components, and (2) measuring reconstruction error as the log-dampened magnitude of complex frequency differences. This differs from existing frequency losses [2, 3] that compute distances using the raw magnitudes of complex differences or separate amplitude/phase components.

For training, we work with pairs of low-resolution (LR) and high-resolution (HR) images. We aim to infer the HR image from its LR observation. We apply the 2D discrete fast Fourier transform (FFT) with orthonormal normalization to the predicted and ground-truth representations, converting spatial representations $f(x, y)$ into their frequency domain counterparts $\mathcal{F}(u, v)$. For each frequency component at position (u, v) , we decompose its complex Fourier value into real (Re) and imaginary (Im) parts. Following the FFL distance formulation of [3], this decomposition preserves both amplitude and phase information. We first compute log-space differences between the ground-truth $\mathcal{F}_{\text{target}}$ and the predicted image $\mathcal{F}_{\text{pred}}$ as:

$$\begin{aligned} \Delta_{\text{Re}}(u, v) &= \log |\text{Re}(\mathcal{F}_{\text{pred}}) + \epsilon| - \log |\text{Re}(\mathcal{F}_{\text{target}}) + \epsilon| \\ \Delta_{\text{Im}}(u, v) &= \log |\text{Im}(\mathcal{F}_{\text{pred}}) + \epsilon| - \log |\text{Im}(\mathcal{F}_{\text{target}}) + \epsilon| \end{aligned} \quad (1)$$

where $\epsilon = 10^{-8}$ is used for numerical stability.

These log-difference maps are combined into an adaptive weight map that emphasizes frequencies with larger discrepancies as:

$$w_{\text{rel}}(u, v) = \left(\sqrt{\Delta_{\text{Re}}^2 + \Delta_{\text{Im}}^2} \right) \quad (2)$$

To compute the loss, we also measure the log-dampened reconstruction error:

$$D_{\log}(u, v) = \log (|\mathcal{F}_{\text{pred}}(u, v) - \mathcal{F}_{\text{target}}(u, v)| + 1) \quad (3)$$

Logarithmic dampening ensures that errors are evaluated on a compressed scale across the wide dynamic range of frequency amplitudes. The gradient with respect to the predicted frequency coefficients satisfies:

$$\left| \frac{\partial D_{\log}}{\partial \mathcal{F}_{\text{pred}}} \right| \propto \frac{1}{|\mathcal{F}_{\text{pred}} - \mathcal{F}_{\text{target}}| + 1} \quad (4)$$

This inverse relationship means that smaller errors receive proportionally stronger gradient signals than larger ones, preventing high-amplitude background-based reconstruction errors from overwhelming the optimization.

Our proposed Log Focal Frequency Loss (LFFL) is defined as:

$$\mathcal{L}_{\text{LFFL}} = \frac{1}{MN} \sum_{u=0}^{M-1} \sum_{v=0}^{N-1} w_{\text{rel}}(u, v)^\alpha \cdot D_{\log}(u, v) \quad (5)$$

where $\alpha > 0$ is a ‘‘focal’’ scaling factor that controls emphasis on relatively harder frequencies.

When manipulating Fourier coefficients, the DC component (at $(u, v) = (0, 0)$ and equal to the average value of the image) requires specific care. In our implementation, we zero out the DC components of $\mathcal{F}_{\text{pred}}$ and $\mathcal{F}_{\text{target}}$ for computing the weight map w_{rel} , which effectively excludes the DC component from contributing to the loss.

2.2. Overall Training Loss

In our GAN architecture, the Generator training loss combines standard spatial losses (pixel-level, perceptual, adversarial) with our proposed LFFL term as:

$$\mathcal{L}_{\text{total}} = \lambda_1 \mathcal{L}_{\text{pixel}} + \lambda_2 \mathcal{L}_{\text{perc}} + \lambda_3 \mathcal{L}_{\text{adv}} + \lambda_4 \mathcal{L}_{\text{LFFL}} \quad (6)$$

where $\lambda_1, \lambda_2, \lambda_3$, and λ_4 constitute weight factors for the L1 pixel-wise loss, a VGG-based perceptual loss [5], an adversarial loss, and our proposed LFFL, respectively. The adversarial loss follows the relativistic average GAN formulation [8]. Specific weight factor values are provided in Section 3.2.

2.3. Selection of Frequency Content for LFFL

We compute LFFL on the FFT of different input spatial representations depending on the restoration task. For **deblurring**, we apply LFFL to the perceptual features extracted from VGG-19 [9] layer `conv1_2`. Early VGG layers capture information such as edges and textures, which aligns well with the restoration goal. For **denoising**, we compute LFFL directly on image intensities to preserve fidelity to the raw signal, ensuring genuine high-frequency structural details are retained.

3. EXPERIMENTS

3.1. Datasets

We evaluate our method on two fluorescence microscopy datasets with varying acquisition characteristics and degradation types, aiming to illustrate the capacities of our proposed LFFL loss in deblurring and denoising tasks:

- **Deblurring: Out-of-focus deformed nuclei dataset (in-house).** This use-case focuses on fluorescence microscopy images of fibroblast cells stained for lamin A/C to delineate the nuclei. The cells were cultured on microgroove substrates to induce 3D nuclear deformations [10]. The dataset contains 945 image pairs

Table 1. Quantitative comparison of spatial and frequency-domain losses on fluorescence microscopy datasets. Bold indicates best mean result per metric. * indicates statistical significance ($p < 0.001$, paired t-test) compared to the best baseline metric.

Method	Out-of-focus deformed nuclei (N=877)						Noisy zebrafish embryo (N=600)					
	PSNR \uparrow	SSIM \uparrow	LPIPS \downarrow	FID \downarrow	FSIM \uparrow	GMSD \downarrow	PSNR \uparrow	SSIM \uparrow	LPIPS \downarrow	FID \downarrow	FSIM \uparrow	GMSD \downarrow
Spatial only	36.297	0.876	0.0175	30.146	0.929	0.0727	33.675	0.897	0.245	93.434	0.919	0.0503
FFL [3]	35.934	0.872	0.0177	31.002	0.929	0.0731	33.793	0.900	0.241	93.559	0.920	0.0492
FSL [2]	35.748	0.866	0.0190	32.449	0.924	0.0780	33.737	0.899	0.248	91.077	0.920	0.0501
LFFL ($\alpha = 0.5$)	36.184*	0.885*	0.0157*	29.345	0.937*	0.0699*	34.118*	0.911*	0.266	98.848	0.921*	0.0488*
LFFL ($\alpha = 1$)	36.674*	0.883*	0.0173	28.169	0.933*	0.0706*	34.142*	0.910*	0.266	95.958	0.917	0.0505
LFFL ($\alpha = 2$)	36.856*	0.889*	0.0166*	37.111	0.936*	0.0679*	34.163*	0.911*	0.274	95.926	0.914	0.0515

(of size $2,044 \times 2,048$ pixels) acquired at a resolution of $0.33 \mu\text{m}/\text{pixel}$ using a 20X microscope objective. Low-resolution images were acquired with a defocus of $\pm 5 \mu\text{m}$ from the optimal focal plane.

- **Denoising: Noisy zebrafish embryo dataset (open-access).** This use-case focuses on fluorescence microscopy images of EGFP-labeled zebrafish embryos from the FMD dataset [11]. It contains 1,000 image pairs (of size 512×512 pixels) with real noisy observations and corresponding averaged ground-truth denoised images.

We split each dataset into training and test sets at the highest hierarchical level (experiment or FOV) to prevent data leakage, targeting a 40%/60% ratio.

3.2. Implementation Details

We use a 16-layer RRDB Generator from ESRGAN [12] and a PatchGAN Discriminator [13]. We extract patches of size 256×256 pixels from regions of interest and normalize patch intensity values to $[0,1]$ using the bit depth for the maximal value. This yields 1,440 patches from the nuclei dataset and 1,000 patches from the zebrafish dataset. Loss weights were empirically set to: $\lambda_1 = 0.1$ for deblurring, $\lambda_1 = 1$ for denoising, $\lambda_2 = 1$, and $\lambda_3 = 0.005$. The weight factor λ_4 for frequency-domain loss $\mathcal{L}_{\text{LFFL}}$ was calibrated per model to achieve comparable initial gradient magnitudes and remained fixed during training. For our three models with $\alpha \in \{0.5, 1, 2\}$, we set $\lambda_4 \in \{2, \sqrt{2}, \sqrt[4]{2}\}$ for deblurring and $\lambda_4 \in \{4, 2, \sqrt{2}\}$ for denoising, following an inverse relationship with α .

The perceptual loss uses `conv2_2` layer features from a VGG-19 pretrained on ImageNet. We use AdamW optimizer with $\beta_1 = 0.9$, $\beta_2 = 0.999$, learning rates of 10^{-4} (Generator) and 10^{-5} (Discriminator), with dynamic Discriminator scheduling for training stability. Models were trained for 200 epochs with batch size 4.

3.3. Evaluation Metrics

We evaluate PSNR, SSIM, FSIM [14], and GMSD [15] at the patch level for the zebrafish dataset and at the nuclear level for the nuclei dataset, where we extract nuclear bounding-boxes

using masks from Cellpose [16]. LPIPS-VGG [17] is reported at the patch level and FID [18] at the dataset level.

3.4. Benchmark Methods

We compare LFFL against three baselines: spatial baseline ($\mathcal{L}_{\text{pixel}}$, $\mathcal{L}_{\text{perc}}$, and \mathcal{L}_{adv} only), FFL [3], and FSL [2] excluding their Fourier Discriminator to isolate loss contributions¹. All methods use identical training/test sets, architectures and training configurations. FFL and FSL are computed on image FFTs as described in their respective papers, with weights calibrated to match LFFL’s initial gradient magnitudes.

4. RESULTS

Results for deblurring and denoising are reported in Table 1. The proposed LFFL consistently outperforms spatial and frequency-domain losses on the deblurring task across all metrics. For denoising, where pixel-level fidelity is more critical, LFFL achieves gains in PSNR and SSIM while maintaining competitive perceptual performance. The more modest improvements for denoising may be attributed to imperfect ground-truth images, which contain residual noise that limits the effectiveness of frequency-domain supervision.

Figure 1 shows some visual restoration results. For deblurring, LFFL recovers cleaner nuclear boundaries with fewer artifacts and more faithful subcellular textures while maintaining overall structural coherence. Other losses tend to introduce spurious details and boundary irregularities in defocused regions. For denoising, LFFL achieves superior noise suppression with smoother intensity transitions, whereas baseline methods exhibit residual noise manifesting as pixelation and graininess artifacts.

We evaluate the scaling factor α in Eq. 2 across values of 0.5, 1, and 2. For both tasks, $\alpha = 0.5$ yields better perceptual metrics while $\alpha = 2$ achieves higher PSNR/SSIM, reflecting a trade-off between amplifying large relative errors ($\alpha = 2$, aggressive hard-frequency focus) and compressing error magnitudes ($\alpha = 0.5$, reduced sensitivity to large errors).

¹FSL was originally designed to work with a Fourier-domain Discriminator. We evaluate its loss formulation in isolation only to contrast weighting behavior, not to assess the full model’s performance.

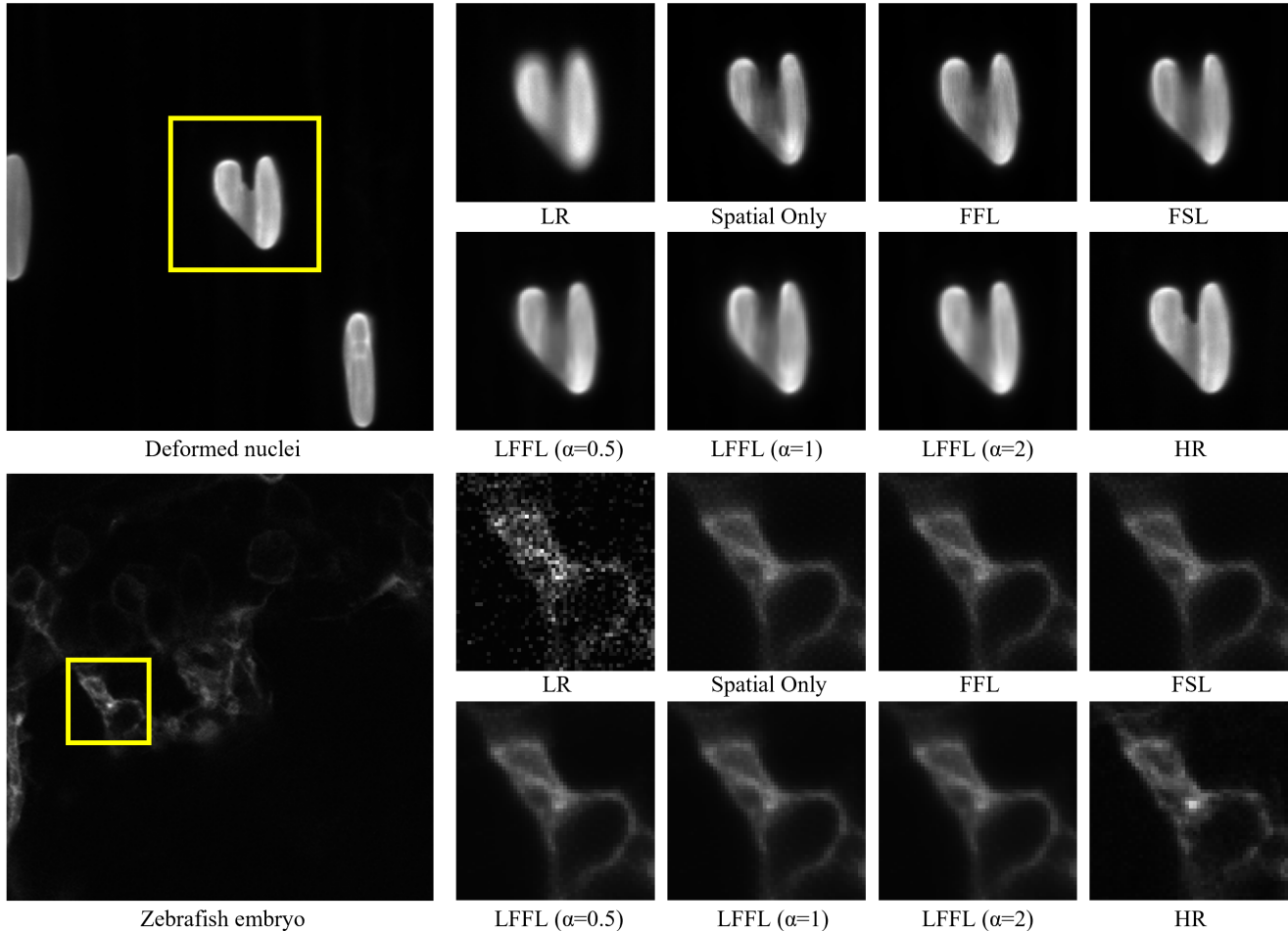


Fig. 1. Visual comparison of deblurring (top) and denoising (bottom) results with magnified regions from yellow boxes.

5. DISCUSSION

Our two-stage logarithmic approach addresses key challenges in frequency-domain supervision for microscopy image restoration. Our adaptive weighting $w_{\text{rel}}(u, v)$ ensures all frequency components receive attention proportional to their reconstruction difficulty rather than their signal strength. Our focal scaling factor α controls this emphasis: smaller values (e.g., $\alpha = 0.5$) compress the weight range for more uniform weights, while larger values (e.g., $\alpha = 2$) increase emphasis on challenging frequencies. Since high-frequency regions can contain both fine structural details and noise artifacts, larger α may amplify residual noise in ground-truth images. In practice, we recommend $\alpha = 1$ as a balanced default, or $\alpha = 0.5$ to prioritize perceptual quality.

Our proposed logarithmic compression decouples loss magnitude from gradient strength: high-amplitude errors contribute more to the total loss but produce proportionally smaller gradients, preventing them from overwhelming optimization and ensuring the network attends to errors across all

frequencies. We compared to alternative frequency-domain losses which face a common challenge: balancing supervision across frequencies with vastly different amplitudes. In FFL [3], both weights and errors scale up with raw amplitude, creating squared or cubic dependency on signal strength. This causes the loss to collapse sharply once low frequencies converge, destabilizing training. FSL [2] avoids weight tuning but also allows high-amplitudes to dominate, limiting fine-detail supervision for restoration tasks.

6. CONCLUSION

We introduced a logarithmic focal frequency loss (LFFL) for microscopy image restoration, addressing foreground-background imbalance and spectral bias. LFFL can be easily integrated into GAN-based frameworks without architectural changes. Experiments show strong structural and perceptual gains for deblurring and improvements in pixel fidelity for denoising, demonstrating its effectiveness and practicality for bioimage restoration and related reconstruction tasks.

7. COMPLIANCE WITH ETHICAL STANDARDS

This study utilized anonymized patient-derived cells provided by clinical collaborators at Aix Marseille University and Marseille Hospital (AP-HM), France, collected under approved institutional protocols. Zebrafish embryo data are made available in open access (MIT license) [11] with no ethical approval requirement.

8. ACKNOWLEDGMENTS

This work is funded in part by an endowment in Cardiovascular Bioengineering from the AXA Research Fund (to A.I.B.) and a doctoral fellowship from Institut Polytechnique de Paris (to X.Z.). The authors thank Prof. Catherine Badens and Dr. Camille Desgrouas for providing cell samples.

9. REFERENCES

- [1] N. Rahaman, A. Baratin, D. Arpit, F. Dräxler, M. Lin, F. A. Hamprecht, Y. Bengio, and A. C. Courville, “On the spectral bias of neural networks,” in *International Conference on Machine Learning*, 2018.
- [2] D. Fuoli, L. Van Gool, and R. Timofte, “Fourier space losses for efficient perceptual image super-resolution,” in *2021 IEEE/CVF International Conference on Computer Vision*, 2021, pp. 2340–2349.
- [3] L. Jiang, B. Dai, W. Wu, and C. C. Loy, “Focal frequency loss for image reconstruction and synthesis,” in *2021 IEEE/CVF International Conference on Computer Vision*, 2021, pp. 13899–13909.
- [4] H. Zhao, O. Gallo, I. Frosio, and J. Kautz, “Loss functions for image restoration with neural networks,” *IEEE Transactions on Computational Imaging*, vol. 3, no. 1, pp. 47–57, Mar. 2017.
- [5] J. Johnson, A. Alahi, and F.-F. Li, “Perceptual losses for real-time style transfer and super-resolution,” in *Computer Vision – ECCV 2016*, 2016, pp. 694–711.
- [6] J. Chen, C. Duanmu, and H. Long, “Large kernel frequency-enhanced network for efficient single image super-resolution,” in *2024 IEEE/CVF Conference on Computer Vision and Pattern Recognition Workshops*, 2024, pp. 6317–6326.
- [7] P. Duan, T. Shan, X. Kang, and S. Li, “Spectral super-resolution in frequency domain,” *IEEE Transactions on Neural Networks and Learning Systems*, vol. 36, no. 7, pp. 12338–12348, 2025.
- [8] A. Jolicoeur-Martineau, “The relativistic discriminator: a key element missing from standard GAN,” in *International Conference on Learning Representations*, 2019.
- [9] S. Liu and W. Deng, “Very deep convolutional neural network based image classification using small training sample size,” in *2015 3rd IAPR Asian Conference on Pattern Recognition*, 2015, pp. 730–734.
- [10] C. Leclech, G. Cardillo, B. Roellinger, X. Zhang, J. Frederick, K. Mamchaoui, C. Coirault, and A. I. Barakat, “Micro-scale topography triggers dynamic 3d nuclear deformations,” *Advanced Science*, vol. 12, no. 11, Jan. 2025.
- [11] Y. Zhang, Y. Zhu, E. Nichols, Q. Wang, S. Zhang, C. Smith, and S. Howard, “A poisson-gaussian denoising dataset with real fluorescence microscopy images,” in *2019 IEEE Conference on Computer Vision and Pattern Recognition*, 2019.
- [12] X. Wang, K. Yu, S. Wu, J. Gu, Y. Liu, C. Dong, Y. Qiao, and C. C. Loy, “Esrgan: Enhanced super-resolution generative adversarial networks,” in *Computer Vision – ECCV 2018 Workshops*, 2019, p. 63–79.
- [13] P. Isola, J.-Y. Zhu, T. Zhou, and A. A. Efros, “Image-to-image translation with conditional adversarial networks,” in *2017 IEEE Conference on Computer Vision and Pattern Recognition*, July 2017, p. 5967–5976.
- [14] L. Zhang, L. Zhang, X. Mou, and D. Zhang, “Fsim: A feature similarity index for image quality assessment,” *IEEE Transactions on Image Processing*, vol. 20, no. 8, pp. 2378–2386, Aug. 2011.
- [15] W. Xue, L. Zhang, X. Mou, and A. C. Bovik, “Gradient magnitude similarity deviation: A highly efficient perceptual image quality index,” *IEEE Transactions on Image Processing*, vol. 23, no. 2, pp. 684–695, Feb. 2014.
- [16] C. Stringer, T. Wang, M. Michaelos, and M. Pachitariu, “Cellpose: a generalist algorithm for cellular segmentation,” *Nature Methods*, vol. 18, no. 1, pp. 100–106, Dec. 2020.
- [17] R. Zhang, P. Isola, A. A. Efros, E. Shechtman, and O. Wang, “The unreasonable effectiveness of deep features as a perceptual metric,” in *2018 IEEE/CVF Conference on Computer Vision and Pattern Recognition*, June 2018.
- [18] M. Heusel, H. Ramsauer, T. Unterthiner, B. Nessler, and S. Hochreiter, “Gans trained by a two time-scale update rule converge to a local nash equilibrium,” in *31st International Conference on Neural Information Processing Systems*, 2017, p. 6629–6640.